

A Letters Journal Exploring the Frontiers of Physics

OFFPRINT

Recurrence-based characterization of model shadowability in the presence of unstable dimension variability

Vitor H. A. Fávaro, Norbert Marwan, Jürgen Kurths, Celso Grebogi and Ricardo L. Viana

EPL, **152** (2025) 61002

Please visit the website
www.epljournal.org

Note that the author(s) has the following rights:
– immediately after publication, to use all or part of the article without revision or modification, **including the EPLA-formatted version**, for personal compilations and use only;
– no sooner than 12 months from the date of first publication, to include the accepted manuscript (all or part), **but not the EPLA-formatted version**, on institute repositories or third-party websites provided a link to the online EPL abstract or EPL homepage is included.
For complete copyright details see: https://authors.epletters.net/documents/copyright.pdf.

A Letters Journal Exploring the Frontiers of Physics

December 2025

EPL, **152** (2025) 61002
doi: 10.1209/0295-5075/ae2cc4

www.epljournal.org

Recurrence-based characterization of model shadowability in the presence of unstable dimension variability

Vitor H. A. Fávaro[1(a)], Norbert Marwan[2], Jürgen Kurths[2,3], Celso Grebogi[4] and Ricardo L. Viana[1,5]

[1] *Universidade Federal do Paraná, Departamento de Física - 81531-980, Curitiba, Paraná, Brazil*
[2] *Potsdam Institute for Climate Impact Research - 14412 Potsdam, Germany*
[3] *Research Institute of Intelligent Complex Systems, Fudan University - Shanghai 200433, China*
[4] *Institute for Complex Systems and Mathematical Biology, King's College, University of Aberdeen Aberdeen AB24 3UE, UK*
[5] *Universidade Federal do Paraná, CICTI, NCC - Curitiba, Paraná, Brazil*

received 15 September 2025; accepted in final form 15 December 2025
published online 29 December 2025

Abstract – Unstable dimension variability is an extreme form of non-hyperbolic behavior, causing severe obstructions to shadowability of numerically generated trajectories of chaotic systems. It has been argued that, in spite of the poor model shadowability of systems with unstable dimension variability, ensembles of chaotic numerical trajectories may still be useful for statistical calculations. The kicked double rotor is a four-dimensional map exhibiting unstable dimension variability for a large parameter interval. By exploring the recurrence properties, we confirm previous claims that, despite the unpredictability of individual trajectories in the kicked double rotor due to unstable dimension variability, statistical measures and recurrence properties remain stable, suggesting their robustness in characterizing the system. While these findings are specific to this system and do not constitute a general proof, a sliding window analysis further confirms the temporal consistency of recurrence measures, supporting their reliability in studying complex chaotic dynamics and encouraging further exploration of their role in hyperchaotic regimes.

Copyright © 2025 EPLA

All rights, including for text and data mining, AI training, and similar technologies, are reserved.

Introduction. – Theoretical physics seeks to understand natural phenomena through mathematical modeling expressed in the form of differential equations and related mathematical systems. In particular, dynamical systems rely on fundamental laws and observational data to build mathematical models, whose solutions are used to analyze, predict, and control the behavior. However, nonlinear models, in general, do not have analytical solutions, in such a way that numerical (computer-generated) solutions are necessary to obtain approximate solutions.

The possibility of chaotic behavior in the numerical solution of a large number of nonlinear dynamical systems poses important questions related to the reliability of computer-generated solutions. This problem arises due to the instability of chaotic orbits to small perturbations, the so-called butterfly effect [1]. In numerical simulations, there are always one-step errors that come from both machine arithmetic round-off and those errors inherent to the numerical algorithms [2], such as Runge-Kutta methods for solving ordinary differential equations [3].

(a) E-mail: vitor.favaro@ufpr.br (corresponding author)

This is the central problem addressed by the concept of model shadowability, which deals with the validity of deterministic modeling of chaotic systems [4,5]. In order to explain the types of modeling difficulties associated with chaotic motion, let us introduce two models of a physical system, named A and B, that are supposedly close to each other. More specifically, if we describe model A by a system $\mathrm{d}\mathbf{x}/\mathrm{d}t = \mathbf{f}(\mathbf{x}, t)$ (in a multidimensional phase space), then model B will be its perturbed version, namely $\mathrm{d}\mathbf{x}/\mathrm{d}t = \mathbf{f}(\mathbf{x}, t) + \boldsymbol{\epsilon}(t)$, where $\boldsymbol{\epsilon}(t)$ is a small time-dependent random perturbation.

In this context, there is model shadowability if (computer-generated) trajectories of model A stay close to some trajectories of model B [5]. In practice, model shadowability for a reasonably large time interval is a necessary requirement for either model to represent a physical system. However, difficulties of different levels affect model shadowability and can be classified into three categories:

i) Firstly, there are minor modeling difficulties if model A is a hyperbolic chaotic system. For them, it can be proved [6,7] that trajectories of model A can always

be shadowed by trajectories of model B for an infinite time τ.

ii) A second category, presenting moderate modeling difficulties, comprises chaotic systems with non-hyperbolic tangencies, *i.e.*, there are tangencies of the stable and unstable manifolds of unstable periodic orbits embedded in an invariant chaotic set (like a chaotic attractor [8]). In those cases, trajectories of model A are shadowed by trajectories of model B by a finite amount of time τ, which scales with model uncertainty as $\tau \sim \epsilon^{-\alpha}$, where $\epsilon = \max|\boldsymbol{\epsilon}(t)|$, and $\alpha \leq 1/2$ is a scaling exponent [9,10].

iii) A third category, of more severe modeling difficulties, concerns chaotic systems displaying a strong form of non-hyperbolic behavior, called unstable dimension variability (UDV). In systems with UDV, the splitting of the phase space into stable and unstable manifolds is not continuous, since there are unstable periodic orbits with different numbers of unstable directions [11], thus violating one of the basic conditions for hyperbolicity of the chaotic invariant set [12–14]. A similar perspective is provided by the concept of heterochaos, proposed by [15]. As a consequence, for systems with UDV, the finite-time Lyapunov exponent closest to zero fluctuates about zero [16–19]. Accordingly, the shadowing time can be estimated as $\tau \sim \epsilon^{-2m/\sigma^2}$, where m and σ^2 are, respectively, the mean and variance of the time-one Lyapunov exponent closest to zero [20,21]. Particularly, if $m \approx 0$, the shadowing time can be extremely small.

Since UDV implies the existence of model shadowability for such short time intervals, it is doubtful if either model is capable of describing a physical system. This issue has been considered by Lai, Grebogi, and Kurths [22], who proposed that, while individual chaotic trajectories may not be shadowable, ensembles of them continue to be useful to compute statistical averages. They considered a typical chaotic system exhibiting UDV, a kicked double rotor, and evaluated the influence of the modeling error ϵ on some physical quantities. They have considered only a particular value of the system parameter, for which they concluded that the modeling error has no significant effect on statistical averages.

In this work, we revisit the work of Lai *et al.* and explore a wider interval of system parameters to investigate the effect of modeling error on these quantities. Moreover, we performe a recurrence-based diagnostics in order to evaluate the influence of the modeling error. Recurrences are important properties of dynamical systems, and their quantitative analysis allows the determination of various measures involving the deterministic content of time series [23–27]. Note that a system with UDV cannot be considered strictly deterministic, in spite of being described by well-defined mathematical equations, since their trajectories, being non-shadowable, cannot be used individually to model real trajectories of the physical system (they have been called pseudo-deterministic for this reason, cf. [5]).

Kicked double rotor. – The first description of UDV in a physically relevant dynamical system is due to Romeiras *et al.* in 1992 [28], who identified this phenomenon in a periodically kicked double rotor. Later on, UDV has been observed in many other dynamical systems [29–33]. It is thought that UDV is actually ubiquitous in multidimensional systems, including spatially extended models of fluids and plasmas [34]. In this section we briefly outline the mathematical model of the kicked double rotor and why it exhibits UDV for a wide range of parameters.

The kicked double rotor consists of two rods with negligible mass and lengths ℓ_1 and $2\ell_2$, respectively, free to move in a plane, without gravity. Particles of mass $m_2/2$ are attached to the ends of a second rod, while a particle of mass m_1 is fixed at the connection between the rods. The system is subjected to an impulsive time-periodic force along a reference direction with amplitude f_0 and period T. Additionally, there are dissipative effects at the joints, which are represented by viscous forces applied to the rods, proportional to the angular velocities $\dot{\theta}_1$ and $\dot{\theta}_2$ with friction coefficients ν_1 and ν_2, respectively.

The equations of motion in this case can be analytically solved in the intervals between two consecutive delta-kicks and in the neighborhood of a given kick. We define discrete variables $(\theta_{1,2})_n$ and $(\dot{\theta}_{1,2})_n$ as the angular positions and velocities just after a kick at time $t = nT$. This yields a four-dimensional dissipative map

$$\mathbf{X}_{n+1} = \mathbf{M}\mathbf{Y}_n + \mathbf{X}_n, \tag{1}$$

$$\mathbf{Y}_{n+1} = \mathbf{L}\mathbf{Y}_n + \mathbf{G}(\mathbf{X}_{n+1}), \tag{2}$$

where we defined the vectors

$$\mathbf{X}_n = \begin{pmatrix} (\theta_1)_n \\ (\theta_2)_n \end{pmatrix}, \quad \mathbf{Y}_n = \begin{pmatrix} (\dot{\theta}_1)_n \\ (\dot{\theta}_2)_n \end{pmatrix}, \tag{3}$$

with the angular positions are defined mod 2π, and the forcing term

$$\mathbf{G}(\mathbf{X}_{n+1}) = f_0 \begin{pmatrix} \frac{1}{\sqrt{2}} \sin(\theta_1)_{n+1} \\ \sin(\theta_2)_{n+1} \end{pmatrix}. \tag{4}$$

For simplicity, we have fixed the values taken on by all the parameters, namely $T = m_1 = m_2 = \nu_1 = \nu_2 = \ell_2 = 1$ and $\ell_1 = 1/\sqrt{2}$, leaving the forcing amplitude f_0 as our control parameter. With these choices the matrices $\mathbf{M}$ and $\mathbf{L}$ have constant elements,

$$\mathbf{L} = \begin{pmatrix} 0.241427723 & 0.272608937 \\ 0.272608937 & 0.514036661 \end{pmatrix}, \tag{5}$$

$$\mathbf{M} = \begin{pmatrix} 0.485963338 & 0.213354400 \\ 0.213354400 & 0.699317739 \end{pmatrix}. \tag{6}$$

The dynamics of the kicked double rotor map has been extensively studied, and here we present an outline of the results of interest to our numerical investigation. Due to

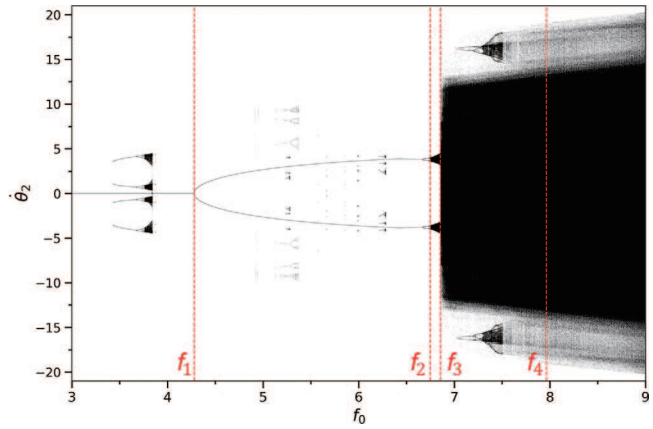


Fig. 1: Bifurcation diagram of $\dot{\theta}_2$ *vs.* the control parameter f_0. Red dashed lines indicate significant transitions: f_1 (period-doubling of $\mathbf{P}$), f_2 (2-band chaotic attractor), f_3 (onset of UDV), and f_4 (maximum of UDV).

the symmetry of the map equations under the transformations $\mathbf{X} \to -\mathbf{X}$ and $\mathbf{Y} \to -\mathbf{Y}$, there is an invariant subspace about the fixed point $\mathbf{0} = (0, 0, 0, 0)$. Another fixed point is $\mathbf{P} = (\pi, \pi, 0, 0)$. For small values of f_0, the latter undergoes a period-doubling bifurcation at $f_0 = f_1 \approx 4.28$, yielding a stable period-2 orbit, coexisting with many other periodic and chaotic attractors.

As illustrated in the bifurcation diagram for $\dot{\theta}_2$ as a function of f_0 in fig. 1, increasing the parameter f_0 leads the system through a period-doubling cascade, generating a 2-band chaotic attractor at $f_0 = f_2 \approx 6.7469$. The chaotic bands merge into a single chaotic band, at $f_0 = f_3 \approx 6.85425150$ due to an interior crisis triggered by the collision of the two-band chaotic attractor with a period-6 unstable orbit. We thus have a pre-critical attractor A, for $f_1 < f_2 < f_3$, and a post-critical attractor B for $f_0 > f_3$.

The dynamical structure of the pre- and post-critical attractors was investigated by Kubo *et al.* [19]. Through direct computation of the eigenvalues of the tangent map $\mathbf{DF}$, they identified saddle orbits embedded in A with unstable dimension $d_u = 1$ and stable dimension $d_s = 3$. In addition, unstable orbits with $d_u = 2$ and $d_s = 2$ were found outside A. These orbits are engulfed by the post-critical attractor B and become part of it, which characterizes UDV, since the post-critical attractor contains orbits with both $d_u = 1$ and $d_u = 2$. Moreover, the onset of UDV occurs at f_3, reaching its maximum at $f_4 \approx 7.9632$, where the shadowing time attains its lowest possible value [35].

Effects of modeling error. – The lack of model shadowability due to UDV represents an almost insurmountable problem for assessing the goodness of computer-generated trajectories. If this fact is taken without further criticism, it might well happen that the mathematical model itself would be useless to describe the dynamics, at least in the parameter ranges where UDV is present (and particularly where it is the most intense).

This fundamental question was addressed by Lai *et al.* [22], who claimed that, although individual trajectories may diverge rapidly due to shadowing breakdown, ensemble-based statistical quantities can remain robust and meaningful in non-hyperbolic regimes. The basis for this reasoning is the fact that statistical predictions using averages for initial conditions use randomly chosen trajectories in the system phase space. As long as the system presents UDV, the trajectories, although deterministic in nature, exhibit an almost stochastic behavior, which can be used to compute averages and fluctuations of quantities of physical interest.

Accordingly, Lai *et al.* [22] considered the kicked double rotor as an example, in the sense that the modeling error ϵ is simulated by adding a term with amplitude ϵ to the external kicks, in the following way:

$$\mathbf{X}_{(n+1)} = \mathbf{M}\mathbf{Y}_{(n)} + \mathbf{X}_{(n)}, \tag{7}$$

$$\mathbf{Y}_{(n+1)} = \mathbf{L}\mathbf{Y}_{(n)} + \mathbf{G}(\mathbf{X}_{(n+1)}) + \epsilon\mathbf{H}(\mathbf{X}_{(n+1)}), \tag{8}$$

where $\epsilon \ll f_0$ is the modeling error, and the perturbation matrix is defined by $\mathbf{H}(\mathbf{X}_{(n+1)}) = [\alpha_1 \sin(\theta_1)_{n+1},\ \alpha_2 \sin(\theta_2)_{n+1}]^\top$, with α_1 and α_2 given as two random variables uniformly distributed in the interval $[0, 1]$. Note that it is necessary that the modeling error be bounded, so as to exclude unbounded random variables, such as those generated by Gaussian or Lorentzian distributions, for example.

Once we choose a value of the modeling error ϵ, we compute quantities of statistical interest like the average energy $\langle E \rangle$ of the system at given (discrete) time n

$$\langle E(n) \rangle = \frac{1}{N} \lim_{N\to\infty} \sum_{n=1}^{N} \left\{ \frac{1}{2} \left[(\dot{\theta}_1)_n^2 + (\dot{\theta}_2)_n^2 \right] + \frac{1}{\sqrt{2}} \left[\cos(\theta_1)_n + \cos(\theta_2)_n \right] \right\}, \tag{9}$$

and, in a similar way, the next three statistical moments: variance $\langle (\Delta E)^2 \rangle$, skewness, and kurtosis.

The analysis of $\langle E \rangle$ and the other moments is performed by numerically iterating the system for different values of the control parameter f_0. The code is implemented in Julia and varies f_0 from 6.5 to 10 with a step size of 10^{-3}. For each value of f_0, we used trajectories of $n = 10^8$ points, discarding the first 10^7 points as transients. The work of Lai *et al.* [22] focused on the value of $f_0 = f_4$ for which UDV is the most intense. In this work, we extend this analysis to a wider range of the control parameter to investigate the effects of both modeling errors and variations in the control parameter on statistical quantities related to the energy of the kicked double rotor.

Figure 2(a) depicts, in a colormap, the dependence of the average energy $\langle E \rangle$ on the values of the control parameter f_0 and the modeling error ϵ. For small values of f_0, including the onset of chaos at $f_2 \approx 6.75$, the average energy increases slightly to ~ 30. However, at $f_0 \approx 7.0$

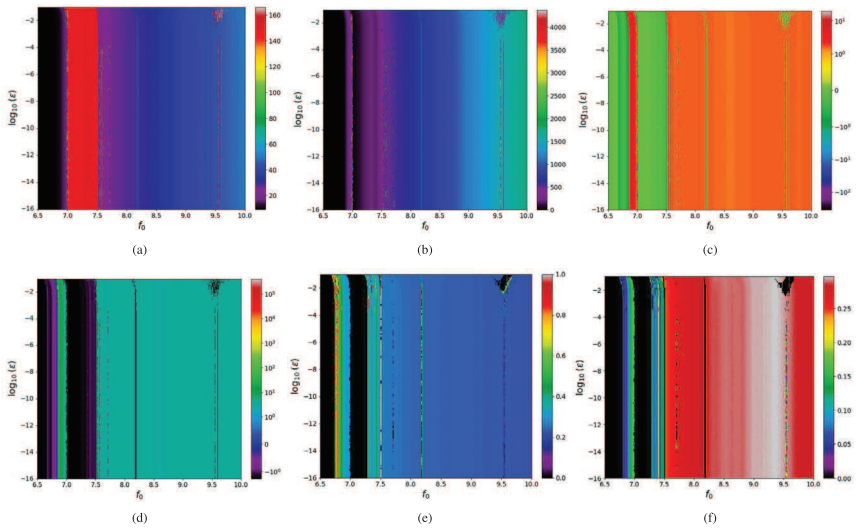


Fig. 2: Colormap of the (a) average energy, (b) variance, (c) skewness, (d) kurtosis, (e) determinism, and (f) laminarity as a function of the modeling error ε and the control parameter f_0. The color scale in each panel shows the magnitude of the corresponding quantity, highlighting how these measures change across parameter space and with modeling error.

to 7.5 the energy increases abruptly at values ~ 150, a fact already noted by Lai *et al.*, who reported a periodic window in this interval, where transient chaos accounts for the observed fluctuations, ending at ~ 7.5.

However, we additionally observe that, around $f_0 \sim 7.0{-}7.5$, the two largest Lyapunov exponents decrease, while the two smallest ones increase, indicating a transient reduction in the divergence rate of nearby trajectories. Similar trends were reported by Lai *et al.* (see fig. 1 in ref. [22]), although they did not discuss these variations in detail. We extend these findings by combining the Lyapunov spectrum with the bifurcation diagram of $\dot{\theta}_2$ (fig. 1), which exhibits signatures of a crisis within the specified interval, as also observed in other diagrams. Moreover, these observations align with the abrupt increase in average energy (fig. 2(a)), suggesting that the system explores new regions of phase space during this interval.

Moreover, the variance $\langle(\Delta E)^2\rangle$ (which is a measure of the energy fluctuations) also has a sudden drop at $f_0 \sim 7.0$ (fig. 2(b)). These fluctuations are due to the finite length of the chaotic trajectories. Assuming a Gaussian dependence, such fluctuations are expected to decrease as $N^{-1/2}$, where N is the trajectory length.

Beyond $f_0 \sim 7.5$, both first Lyapunov exponent and the average energy in the kicked double rotor increases for almost all further values of the forcing amplitude f_0. However, due to the dissipative nature of the system, the average energy is bounded and takes on values until ~ 60. Lai *et al.* have computed an average energy of 28.3565 at $f \approx 8.0$, which is near the point where UDV is the most pronounced, namely $f_4 = 7.9632$, due to the onset of hyperchaos through a blowout bifurcation [36]. Finally, sudden changes are also seen in the higher energy moments, the skewness and kurtosis, at f_2, and around 7.0 to 7.5 (fig. 2(c) and (d)).

To test the robustness of these statistical measures, we varied the modeling error over 15 orders of magnitude, from 10^{-1} to 10^{-16}, representing various sources of uncertainty such as numerical precision and truncation algorithms. The average energy and all their higher moments are not affected by the modeling error, not even when the UDV is the most pronounced, at $f_4 = 7.9632$. This observation confirms the conjecture of Lai *et al.* that such statistical invariants take on the same value over a variation of the modeling error over many decades. Exceptions can be observed for $f_0 \sim 9.4$ to 9.6, and $\epsilon \sim 10^{-1}$ to 10^{-2}, since at these values there could be a periodic window (we expect an infinite number of them but they are typically too narrow to be seen in the figures).

Although individual trajectories in systems with UDV are unpredictable and fail to be shadowable, our results in figs. 2(a)–(d) confirm that the statistical metrics (average, variance, skewness, and kurtosis) remain stable despite model uncertainty. This stability suggests that these measures can be reliably used for characterization, as they do not depend on individual trajectories. However, these results were obtained for a specific case and do not constitute a rigorous proof of the claimed robustness to random perturbations. Thus, further investigation is needed to understand the interplay between uncertainty and statistical stability.

Recurrence-based quantities. – To complement the statistical analysis of the kicked double rotor map, we employ recurrence-based measures used to characterize its dynamical behavior. As aforementioned, these measures will be tested for robustness under small perturbations due to modeling error. Recurrence methods also reveal the system's dynamical structure by identifying recurrent states in phase space and extracting statistical properties from their patterns [25,37].

Let $\mathbf{x}_i = [(\theta_1)_i, (\theta_2)_i, (\dot{\theta}_1)_i, (\dot{\theta}_2)_i]$ represent the state of the system at time i, where $i = 0, 1, 2, \ldots, N$. The elements of the recurrence matrix are defined by

$$R_{i,j} = \Theta(r - \|\mathbf{x}_i - \mathbf{x}_j\|), \tag{10}$$

where $R_{i,j}$ is a binary matrix indicating whether the state $\mathbf{x}_j$ at time j is within an r-neighborhood of the state $\mathbf{x}_i$ at time i [25,26]. This results in $R_{i,j} = 1$ if $\|\mathbf{x}_i - \mathbf{x}_j\| \leq r$, and $R_{i,j} = 0$ otherwise. The function $\Theta(x)$ is the Heaviside function, and $||\cdot||$ denotes a chosen norm. In our case, we used the maximum norm [38].

Given the recurrence matrix, we compute five basic main recurrence-based measures: determinism, laminarity, frequency distribution of recurrence time as estimated by the white vertical lines v ($P_w(v)$), mean recurrence time [39], and the recurrence time entropy [38,40–42].

Given these recurrence-based quantification measures, we considered recurrence plots obtained from time series of eqs. (7) and (8) by randomly choosing the initial conditions in the interval $0 \leq \theta_{1,2} \leq 2\pi$ and $\dot{\theta}_{1,2} = 0$, and considering trajectories with 10^8 iterations, discarding the first 5×10^7 points. We choose the recurrence threshold r by fixing the recurrence rate at 10%, meaning that 10% of all pairs of states in the phase space are recurrent. Smaller values of r reduce point density in recurrence plots, allowing better detection of small variations, whereas larger values increase density but decrease sensitivity to these subtle changes. The recurrence measures are calculated using the `pyunicorn` [43] library in Python. Computations are performed for different values of the control parameter f_0, ranging from 6.5 to 10, with an adaptable step size.

Following the same approach used for the statistical measures in figs. 2(a)–(d), we computed the determinism and laminarity measures for eqs. (7) and (8), varying both the control parameter f_0 and modeling error ϵ. In contrast, the remaining recurrence quantifiers were calculated for eqs. (1) and (2). Figures 2(e), (f) shows the dependence of determinism and laminarity on these parameters. The color map for determinism (fig. 2(e)) reveals that, despite some localized variations observed for specific values of f_0 and ϵ, determinism remains relatively stable across most values of model uncertainty, demonstrating that the recurrence structure persists even with the sensitivity of individual trajectories due to UDV.

Moreover, as shown in fig. 2(e), determinism remains zero until approximately $f_0 \approx 6.75$. This behavior stems from maintaining the recurrence rate at 10%, since determinism is defined as the fraction of recurrence points that lie on diagonal lines of length l_{min} (in our case, $l_{min} \geq 2$) relative to all recurrence points. At such a low recurrence rate, the plot consists mostly of isolated points without continuous diagonal segments of length ≥ 2, so the determinism is zero by definition.

Similarly, fig. 2(f) suggests that the laminarity also remains resilient to increasing model uncertainty, although some parameter regions exhibit fluctuations. Hence, even though the model may be perturbed by modeling error,

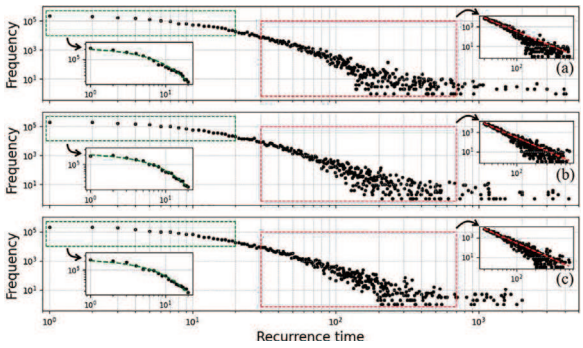


Fig. 3: Statistical distribution of recurrence time v for $f_0 = 7.96$ at three temporal windows: (a) early (window 1), (b) mid-term (window 5000), and (c) late (window 10000).

the core recurrence properties remain unchanged, in accordance with the findings of the previous section. In addition, applying the same reasoning used for fig. 2(e), laminarity remains zero up to $f_0 \approx 6.8$. This occurs because laminarity quantifies the fraction of recurrence points that form vertical lines of length v_{min} (in our case, $v_{min} \geq 2$). At a recurrence rate of 10%, the longest vertical runs are isolated single points, which do not satisfy the v_{min} requirement and, therefore, the laminarity is zero.

Although the determinism and laminarity measures generally take the same value over a wide range of modeling errors, we observe that for $f_0 \sim 9.4$ to 9.6, and $\epsilon \sim 10^{-2}$ to 10^{-1}, there is a structure that slightly deviates from this behavior and is also detected in the statistical measures (figs. 2(a)–(d)).

In order to examine a possible evolution of recurrence properties along the time series, we considered a sliding window that moves over time series segments of 5×10^3 iterations, resulting in a total of 10^4 segments (without overlapping). By shifting these windows across the time series, we determine the statistical distribution of recurrence time v for each window $P_w(i, v)$. Figure 3 presents the distribution of recurrence time for three selected time intervals (similar conclusions can be drawn for other windows as well).

The three panels exhibit qualitatively similar behavior, showing a decreasing frequency with increasing v, which reveals that short quiescent episodes are predominant throughout the time series (fig. 3). The insets highlight that small values of v are well fitted by an exponential decay (green region), of the form e^{-kv}, while for larger intervals (red region), the distribution is better described by a power law $v^{-\alpha}$. Across all analyzed windows, we set $k = 0.126 \pm 0.004$ and $\alpha = 2.896 \pm 0.086$, while the insets serve to illustrate these behaviors. This transition suggests the presence of intermittent dynamics in which short-duration quiescent phases occur much more frequently than longer ones. Moreover, similar patterns have also been observed in the context of noisy on-off intermittency and unstable dimension variability [44].

Subtle differences can be observed in the tails of the distributions across the three windows. The distributions

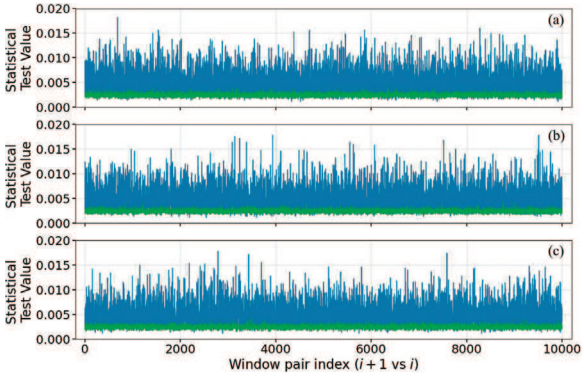


Fig. 4: Statistical Kolmogorov-Smirnov test (blue curves) and mutual information analyzis (green curves) for selected model control parameter: (a) $f_0 = 7.95$, (b) $f_0 = 7.96$, and (c) $f_0 = 7.97$.

in fig. 3(a) and (b) appear to have longer and smoother tails compared to panel (c), possibly indicating a relatively higher occurrence of long quiescent episodes in the earlier parts of the time series. In contrast, the more irregular tail in panel (c) may reflect a transition in the system's dynamics over time.

Thus, based on the distribution $P_w(i, v)$ for each i-th window, with $i = 1, 2, 3, \ldots$, we compare consecutive distributions $P_w(i + 1, v)$ and $P_w(i, v)$ through several statistical methods, namely the Kolmogorov-Smirnov (KS) test and mutual information analysis. The former is a non-parametric method that evaluates whether two samples come from the same distribution by measuring the maximum absolute difference between their cumulative distribution functions [45]. Mutual information, on the other hand, quantifies the amount of shared information between two distributions. In this case, it tells us how much knowing the distribution in one window reduces uncertainty about the distribution in the next one, providing a measure of statistical dependence [46].

Our results are shown in fig. 4, where the blue points represent the KS test and green points indicate the mutual information between consecutive windows, both plotted as function of the window index.

The results presented show that both the KS test values and mutual information remain consistently low over time, reflecting the fact that the recurrence distributions between consecutive windows are very similar and that the recurrence properties exhibit relative temporal stability. The values of the mutual information reinforce this interpretation, as it indicates that the recurrence structures in different windows have little dependence on each other.

These findings corroborate the robustness of the recurrence-based measures discussed previously. The small variations detected, particularly through occasional peaks in the KS test values, suggest that while minor fluctuations occur, the overall statistical properties remain stable. It is worth noting that the mutual information analysis shows an even higher level of consistency, with minimal deviations across different control parameter values. This dual evidence from two independent measures strengthens the conclusion that the recurrence properties are not significantly altered by time evolution.

Finally, to verify the temporal stability of recurrence properties, we employ a sliding window approach on the time series. For each window $i = 1, 2, 3, \ldots$, we compute the mean recurrence time $MRT(i)$ and the recurrence time entropy $RTI(i)$. In fig. 5, we construct a first-return plot to compare $MRT(i + 1)$ as a function of $MRT(i)$, and $RTI(i + 1)$ as a function of $RTI(i)$.

As observed in the first-return plots, both the mean recurrence time (fig. 5(a)) and the recurrence time entropy (fig. 5(b)) form concentrated point clouds centered around well-defined average values. This indicates that the distributions of these recurrence-based measures remain statistically stable over time. However, the lack of any discernible structure or alignment along the diagonal suggests that the values across consecutive windows are uncorrelated. Similar analyses were performed for other values of the control parameter f_0, and consistent patterns were found. In all tested cases, recurrence measures preserved their distributions, supporting the notion that the behavior observed at $f_0 = 7.96$ is not an isolated occurrence.

While the absence of long diagonals in this case implies no direct time correlation, the tight clustering of points suggests that the statistical properties of the recurrence measures remain robust. This statistical stationarity indicates that the measures do not exhibit large fluctuations across time windows and are resilient to minor local variations, confirming that the recurrence structures remain consistent under small temporal or dynamical fluctuations.

Taken together, the consistent results across multiple independent measures provide compelling evidence for the robustness of the recurrence-based and statistical indicators used. These findings support the reliability of the recurrence analysis framework in capturing the essential dynamical features of the system. Nonetheless, it should be noted that this evidence is verified to the kicked double rotor map investigated here. While the observed consistency reinforces the methods' applicability to this case, it does not constitute a general proof of robustness across all dynamical systems.

Conclusions. – Our results demonstrate that while individual trajectories in the kicked double rotor are unpredictable due to UDV, basic statistical measures (average, variance, skewness, and kurtosis) and recurrence properties (determinism and laminarity) remain stable. This stability indicates that these measures are suitable for characterizing the system despite the unpredictability of individual trajectories. It is important to note that these results were obtained for a particular dynamical system and do not constitute a rigorous proof of the claimed robustness of the system to random perturbations.

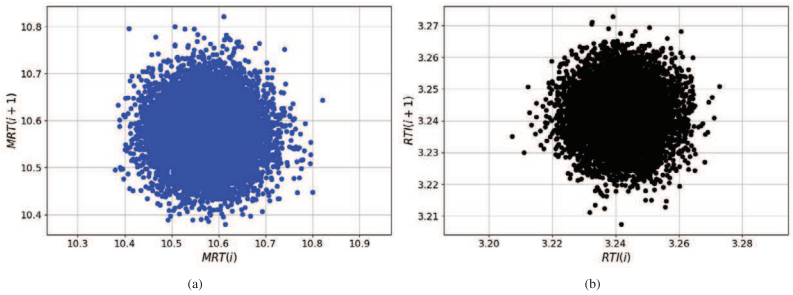


Fig. 5: First-return plots of (a) mean recurrence time $MRT(i)$ and (b) recurrence time entropy $RTI(i)$ for $f_0 = 7.96$, in which each point represents the comparison between the value at window i (horizontal axis) and that at window $i+1$ (vertical axis).

Additionally, the sliding window analysis shows that recurrence properties are temporally consistent, with only minor localized variations. These findings reinforce the reliability of recurrence-based methods for analyzing complex chaotic systems and suggest that further investigation is needed to deepen our understanding of the relationship between statistical stability and recurrence dynamics in hyperchaotic regimes.

To ensure the continuity of our research, we propose investigating whether a relationship exists between the variability of the unstable dimension and the ergodic hypothesis of Statistical Mechanics. Additionally, we aim to examine other statistical invariants of dynamical interest, such as fractal dimensions, to determine whether they also exhibit robustness under small random perturbations of the model.

* * *

The authors acknowledge financial support from the Conselho Nacional de Desenvolvimento Científico e Tecnológico (CNPq, Grant Nos. 403120/2021-7 and 301019/2019-3) and from the Coordenação de Aperfeiçoamento de Pessoal de Nível Superior (CAPES, Grant Nos. 88887.954987/2024-00 and 88881.143103/2017-01).

Data availability statement: The data that support the findings of this study are available upon reasonable request from the authors.

REFERENCES

[1] Lorenz E. N., *J. Atmos. Sci.*, **20** (1963) 130.
[2] Süi E. and Mayers D. F., *An Introduction to Numerical Analysis* (Cambridge University Press) 2003.
[3] Hairer E. *et al.*, *Solving Ordinary Differential Equations I: Nonstiff Problems* (Springer) 1993.
[4] Grebogi C. *et al.*, *Phys. Rev. Lett.*, **65** (1990) 1527.
[5] Poon L. *et al.*, in *Dynamical Systems and Chaos*, edited by Aizawa Y. Saito S. and Shiraiwa K. (World Scientific) 1995, pp. 13–21–.
[6] Bowen R., *J. Differ. Equ.*, **18** (1975) 333.
[7] Viana R. L. *et al.*, *Int. J. Bifurcat. Chaos*, **13** (2003) 3235.
[8] Grebogi C. *et al.*, *J. Complex.*, **3** (1987) 136.
[9] Grebogi C. *et al.*, *Bull. Am. Math. Soc.*, **19** (1988) 465.
[10] Sauer T. and Yorke J. A., *Nonlinearity*, **4** (1991) 961.
[11] Abraham R. and Smale S., *Proc. Symp. Pure Math.*, **14** (1970) 5.
[12] Guckenheimer J. and Holmes P., *Nonlinear Oscillations, Dynamical Systems, and Bifurcations of Vector Fields* (Springer-Verlag) 1983.
[13] Dawson S. P. *et al.*, *Phys. Rev. Lett.*, **73** (1994) 1927.
[14] Lai Y.-C., *Phys. Rev. E*, **59** (1999) R3807.
[15] Saiki Y. *et al.*, *Chaos*, **28** (2018) 103110
[16] Kostelich E. J. *et al.*, *Physica D*, **109** (1997) 81.
[17] Viana R. L. *et al.*, *Phys. Rev. E*, **66** (2002) 046213.
[18] Viana R. L. *et al.*, *Braz. J. Phys.*, **35** (2005) 139.
[19] Kubo G. T. *et al.*, *Phys. Lett. A*, **372** (2008) 5569.
[20] Do Y. and Lai Y.-C., *Phys. Rev. E*, **69** (2004) 016213.
[21] Sauer T. *et al.*, *Phys. Rev. Lett.*, **79** (1997) 59.
[22] Lai Y.-C. *et al.*, *Phys. Rev. E*, **59** (1999) 2907.
[23] Eckmann J.-P. *et al.*, *Europhys. Lett.*, **4** (1987) 973.
[24] Webber C. L. jr. and Zbilut J. P., *J. Appl. Physiol.*, **76** (1994) 965.
[25] Marwan N. *et al.*, *Phys. Rep.*, **438** (2007) 237.
[26] Marwan N., *Eur. Phys. J. ST*, **164** (2008) 3.
[27] Goswami B., *Vibration*, **2** (2019) 332.
[28] Romeiras F. J. *et al.*, *Physica D*, **58** (1992) 165.
[29] Lai Y.-C. and Grebogi C., *Phys. Rev. Lett.*, **82** (1999) 4803.
[30] Lai Y.-C. *et al.*, *Phys. Rev. E*, **60** (1999) 5445.
[31] Viana R. L. and Grebogi C., *Phys. Rev. E*, **62** (2000) 462.
[32] Barreto E. and So P., *Phys. Rev. Lett.*, **85** (2000) 2490.
[33] dos Santos V. *et al.*, *App. Math. Comput.*, **286** (2016) 23.
[34] Galuzio P. P. *et al.*, *Phys. Rev. E*, **84** (2011) 056211.
[35] Sauer T. D., *Phys. Rev. E*, **65** (2002) 036220.
[36] Czajkowski B. M. and Viana R. L., *Chaos, Solitons Fractals*, **184** (2024) 114994.
[37] Marwan N. *et al.*, *Chaos*, **28** (2018) 085601.
[38] Kraemer K. H. *et al.*, *Chaos*, **28** (2018) 085720.
[39] Ngamga E. J. *et al.*, *Phys. Rev. E*, **75** (2007) 036222.
[40] Kraemer K. H. and Marwan N., *Phys. Lett. A*, **383** (2019) 125977.
[41] Slater N. B., *Math. Proc. Cambridge Philos. Soc.*, **46** (1950) 525.
[42] Sales M. R. *et al.*, *Chaos*, **33** (2022) 033140.
[43] Donges J. F. *et al.*, *Chaos*, **25** (2015) 113101.
[44] Viana R. L. *et al.*, *Phys. Rev. E*, **68** (2003) 067204.
[45] Massey F. J., *J. Am. Stat. Assoc.*, **46** (1951) 68.
[46] Kraskov A. *et al.*, *Phys. Rev. E*, **69** (2004) 066138.